ROBUST ESTIMATES OF SEISMIC REFLECTOR ORIENTATIONS WITH WEIGHTED VECTOR DIRECTIONAL FILTER

WEI WANG, JINGHUAI GAO and WENCHAO CHEN

Institute of Wave and Information, School of Electronic and Information Engineering, Xi'an Jiaotong University, 28 Xianning West Road, 710049 Xi'an, P.R. China.
feitianliuhuo@gmail.com, jhgao@mail.xjtu.edu.cn, wencchen@mail.xjtu.edu.cn

(Received March 5, 2010; revised version accepted February 22, 2011)

ABSTRACT

Wang, W., Gao, J. and Chen, W., 2011. Robust estimates of seismic reflector orientations with weighted vector directional filter. *Journal of Seismic Exploration*, 20: 119-134.

A major difficulty in estimating seismic reflector orientations (dip and azimuth) arises at discrete lateral and vertical discontinuities across which reflector dip and azimuth change. To overcome this problem, we explore a weighted vector directional filter (WVDF) for smoothing volumetric dip and azimuth computed by a finite-difference method. The approach falls into three steps: (1) set a reference direction, (2) invert opposite vectors to convert directions into orientations, and (3) smooth the vector field with the WVDF. The smearing and confusing variations that arise across lateral and vertical geological boundaries with traditional dip and azimuth estimations are avoided by the proposed method. This method is more robust for estimating seismic dip and azimuth and has potential for applications such as structure-oriented filtering and coherence. A still more promising application of this method is high-resolution dip and azimuth analysis through volumetric estimations of reflector curvature. Both synthetic and real data examples are used to demonstrate the ability and efficiency of our approach.

KEY WORDS: finite difference, gradient vector, seismic dip and azimuth, vector filter.

INTRODUCTION

Seismic reflector orientation (dip and azimuth) has several applications in seismic data processing and interpretation, such as structure-oriented smoothing (Fehmers and Hocker, 2003; Hoeber et al., 2006; Lavialle et al., 2007), dip-steered coherence (Luo et al., 1996; Marfurt et al., 1998; Gersztenkorn and

0963-0651/11/$5.00

Marfurt, 1999; Marfurt et al., 1999) and curvature attributes estimation (al-Dossary and Marfurt, 2006). Seismic reflector orientation itself provides stratigraphic and geographic information and is a valuable interpretation tool (Dalley, 2008).

Several methods have been proposed to compute the volumetric reflector orientation. One standard scheme for extracting local dips is the local slant stack (Ottolini, 1983). Plane-wave destruction filters are also used to determine dips and are usually followed with smoothing (Fomel, 2002). Besides, instantaneous dip estimation algorithms are also adopted in practice (Barnes, 1996; Luo et al., 1996). They are based on attributes computed from the analytical traces. Since the estimation of instantaneous attributes suffers from singularities when reflector events interfere with each other, Barnes (2000) locally averages instantaneous attributes prior to estimating dip and azimuth, thereby improving stability with only minor lateral resolution loss. Another feasible way to estimate dip and azimuth is the dip scan methods (Marfurt et al., 1998; Marfurt et al., 1999), which calculate coherency attributes over a multiplicity of trial dips, with the dip having the highest coherency measure corresponding to the local dip of the reflector. A disadvantage of the dip-scan approach is that they discretely sample inline and crossline dips so that one may miss subtle features. Moreover, Marfurt (2006) proposes the multiwindow dip scan scheme to avoid the limitations of conventional centered dip and azimuth estimations.

Another solution is to use a Finite-Difference method. It is easy to implement and seismic dips and azimuths are represented by gradient vectors. However, it is a first-derivative operation and therefore tends to amplify high-frequency noise. A smoothing scheme is needed to suppress the noise and extract geological features. It is straightforward to calculate gradient vectors with the finite-difference method, but smoothing this vector field is nontrivial because a seismic event has two opposite normal directions, one of which represents the orientation. For example, both 0° and 180° dips are horizontal events, but their average (90°) is vertical. Therefore, raw directions cannot be taken for a smoothing operation unless some maneuvers are used.

One possible approach to smooth the gradient vector field is the gradient structure tensor method (Randen et al., 2000; Luo et al., 2006). In the method, the gradient structure tensor is constructed by the outer product of the gradient vector with itself and followed by smoothing each element of this tensor individually by a low-pass spatial filter:

$$\mathrm{GST} = \mathrm{LP} * (\mathbf{V}\mathbf{V}^{\mathrm{T}}) = \mathrm{LP} * \begin{pmatrix} (V_x)^2 & V_xV_y & V_xV_z \\ V_yV_x & (V_y)^2 & V_yV_z \\ V_zV_x & V_zV_y & (V_z)^2 \end{pmatrix} . \qquad (1)$$

In eq. (1), $V^T = (V_x,V_y,V_z) = [(\partial U/\partial x),(\partial U/\partial y),(\partial U/\partial z)]$ represents the gradient vector at every point, T denotes the transpose, U is the input data, and LP is a low-pass spatial filter. The eigenvector with the largest eigenvalue will by definition best represent the variability of the seismic data and therefore will be aligned with the vector normal to the reflector events. But the gradient structure tensor approach may fail, when a dominant eigenvalue does not exist and the wrong eigenvector is still selected to determine the reflector orientation (Wang et al., 2008a). In order to avoid inherent instabilities of the gradient structure tensor approach, Wang et al. (2008a) propose an iterative inverse-vector method, which iterates a loop of three steps: (1) set a guide direction, (2) invert opposite vectors, and (3) smooth vectors using an arithmetic average and update the guide. Several iterations are used to update the guide direction progressively to a meaningful average. Although the estimated orientations can be slightly enhanced by this iterative process, lateral and vertical geological boundaries are blurred by the simple Arithmetic Mean Filter (AMF) and cannot be restored in their method. Moreover, these aforementioned smoothing schemes are all centered dip and azimuth estimations with a single analyzing window and they may fail when the analyzing window spans a fault, where they provide at best an estimation of the apparent dip across the fault rather than true reflector dip (Marfurt, 2006).

The edge-preserving filters have been widely used to reduce random noise while preserving the edges. Luo et al. (2002) and AlBinHassan et al. (2006) propose the 2D and 3D edge-preserving smoothing (EPS) algorithms, respectively. However, these edge-preserving methods are designed for scalar seismic data rather than vector data. In order to achieve better preservation of geological boundaries and accurate dip estimations in the vicinity of discontinuities, we propose an edge and detail preserving vector filter, namely weighted vector directional filter (WVDF), for smoothing volumetric dip and azimuth. In this paper, first we apply the enhanced isotropic gradient operator (Wang et al., 2008b) to calculate gradient vectors and then invert them according to the reference direction. Second, the WVDF method is presented to smooth the inversed gradient vector field and to obtain the suitable reflector orientations. We demonstrate the merit of this method through synthetic data and show its efficiency by using real seismic data with a comparison with the AMF method, the instantaneous dip estimation and the dip-scan approach. Finally, we discuss our results and conclude.

GRADIENT VECTOR FIELD COMPUTATION AND INVERSION

For a 3D seismic data U, its gradient at every position X_{ijk} of the grid can be computed by the symmetric finite-difference method:

$$V_x(i,j,k) = (U_{i+1,j,k} - U_{i-1,j,k}) \quad . \tag{2}$$

Alternatively, in this paper, we use the enhanced isotropic gradient operator (Wang et al., 2008b), which is designed to reduce anisotropic inaccuracies of conventional numerical operator such as simple difference, Sobel, and Prewitt, and produce generic frequency-independent operators. In the 2D case, it is

$$V_x(i,j) = (U_{i+1,j} - U_{i-1,j}) + 0.25 * (U_{i+1,j-1} - U_{i-1,j-1} + U_{i+1,j+1} - U_{i-1,j+1}) \quad . \quad (3)$$

In the 3D case, it is

$$\begin{aligned} V_x(i,j,k) = {} & (U_{i+1,j,k} - U_{i-1,j,k}) \\ & + 0.245 * (U_{i+1,j-1,k} - U_{i-1,j-1,k} + U_{i+1,j+1,k} - U_{i-1,j+1,k}) \\ & + 0.245 * (U_{i+1,j,k-1} - U_{i-1,j,k-1} + U_{i+1,j,k+1} - U_{i-1,j,k+1}) \\ & + 0.085 * (U_{i+1,j-1,k-1} - U_{i-1,j-1,k-1} + U_{i+1,j+1,k-1} - U_{i-1,j+1,k-1}) \\ & + 0.085 * (U_{i+1,j-1,k+1} - U_{i-1,j-1,k+1} + U_{i+1,j+1,k+1} - U_{i-1,j+1,k+1}) \quad . \quad (4) \end{aligned}$$

It can be computed in a similar way for the other two components V_y and V_z of the gradient vector V.

As discussed previously, the raw gradient vectors cannot be smoothed directly unless directions are converted into orientations. Therefore, we need first to define a reference direction. We choose the downward vector corresponding to zero dip as the reference direction, which is equivalent to horizontal seismic reflectors (Fig. 1). Then every vector is compared with the reference vector, and if the angle between them is greater than $\pi/2$, the vector is inverted by multiplying each component by -1. The regularized vectors pointing to the downward half space can now be candidates for the smoothing operation.

WEIGHTED VECTOR DIRECTIONAL FILTER

Vector filters are very popular in the color image processing community (Lukac et al., 2005), e.g., Vector Median Filter (VMF), Basic Vector Directional Filter (BVDF). The BVDF refers to the directional information of input vectors and is essentially the directional median filter. Thus, the BVDF is suitable for smoothing the inverted gradient vector field, especially in the vicinity of discontinuities where the BVDF can reduce confused variations and keep geological boundaries less smeared (see later synthetic data examples).

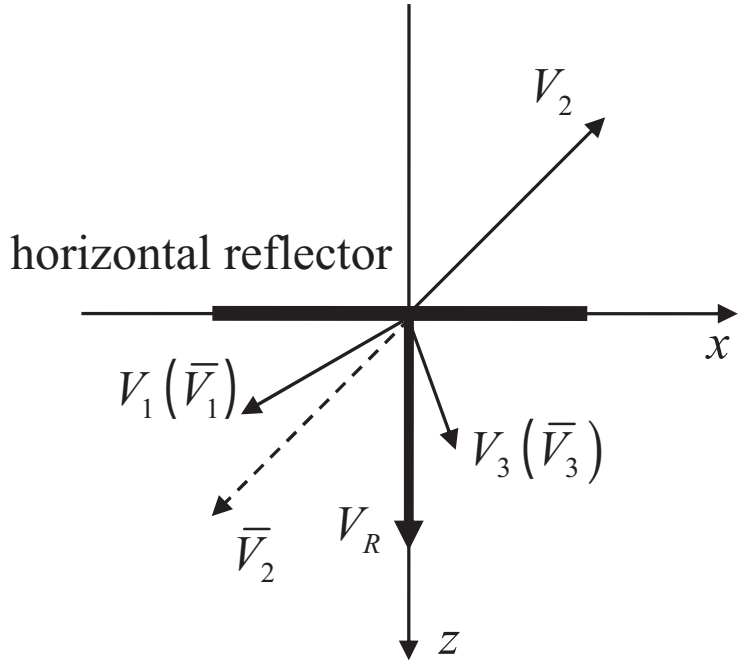

Fig. 1. Gradient vector inversion according to the reference direction V_R.

However, when noisy data and complex geological environments are encountered, the vectors in an analyzing window could be all contaminated. Thus, the BVDF may produce spatially less consistent results because the BVDF seeks one of the input vectors as its output which may be also contaminated. Herein, we propose a weighted average vector filter, i.e., the WVDF, to smooth the inverted gradient vector field.

Consider a cubic window W of size $N_x \times N_y \times N_z$ in the 3D data cube (a square window of size $N_x \times N_z$ or $N_y \times N_z$ in the 2D case) containing the target point at its center. The input gradient vectors inside the window W are denoted as $\bar{V}_j = (\bar{V}_x^j, \bar{V}_y^j, \bar{V}_z^j)$, where $j = 1,2,\cdots,N$, where $N = N_x \times N_y \times N_z$ ($N = N_x \times N_z$ or $N_y \times N_z$ in the 2D case). The general form of the WVDF proposed here is given as a weighted average of the input vectors inside the window W:

$$\bar{V} = \sum_{j=1}^{N} w_j \bar{V}_j = \sum_{j=1}^{N} [\mu_j / \sum_{j=1}^{N} \mu_j] \bar{V}_j \quad , \tag{5}$$

where μ_j is the weighting coefficient of the vector $\bar{V}_j$ and w_j is the normalized version of μ_j, and $\bar{V}$ is the output of the WVDF at the target point.

According to (5), the proposed output is a weighted average of all the vectors inside the filtering window. The weighting coefficients are transforms of the summation of distances between the considered vector and all input vectors inside the filtering window. To smooth seismic dip and azimuth, it is desirable to perform smoothing on all vectors which are from the same most centrally located set. Thus, the adaptive weights should represent the confidence that the vectors under consideration come from the same set. It is, therefore, reasonable to make the weights in (5) proportional to the difference in terms of a distance measure between a given vector and its neighbors inside the filtering window. The design objective is: "*Assign the maximum weight to the vector which is the most centered inside the analyzing window*". Thus, the vector with the maximum weight will be the one which has the minimum distance from all the other vectors. In this way, atypical vectors arising from noise or differently oriented reflectors secondarily covered by the current filtering window will be assigned smaller weights and will contribute less to the final output.

In our WVDF method, we propose to use the vector angle criterion as distance measure. This criterion considers the angle between two vectors as their distance:

$$\alpha(\bar{V}_i,\bar{V}_j) = \cos^{-1}[\bar{V}_i^T\bar{V}_j/(|\bar{V}_i||\bar{V}_j|)] \quad . \tag{6}$$

And the aggregated distance associated with the vector $\bar{V}_j$ inside the filtering window W is defined as follows:

$$A_j = [\sum_{i=1}^{N} \alpha(\bar{V}_i,\bar{V}_j)]/N \quad . \tag{7}$$

The distance A_j falls in $[0,\pi]$ and depicts the deviation of the vector $\bar{V}_j$ from all other vectors in the filtering window. This criterion was first introduced by Trahanias and Venetsanopoulos (1993) to measure distances among RGB color vectors for image processing purposes. In our WVDF method, it is used to measure the angle distances between inverted gradient vectors.

The weighting transform is essentially a membership function with respect to the specific window element. In accordance to our design objective it is reasonable to select an appropriate weighting transform so that the vector with the minimum aggregated angular distance is assigned the maximum weight and vice versa. Thus, an S-shaped monotonically decreasing function can be taken as the membership function. In our WVDF method, the weight μ_j associated with the vector $\bar{V}_j$ takes the following form:

$$\mu_j = R^{\lambda-1}(\pi - A_j)^{\lambda}/[R^{\lambda-1}(\pi - A_j)^{\lambda} + (1 - R)^{\lambda-1}(A_j)^{\lambda}] \quad , \tag{8}$$

where R $\in$ (0,1) is the inflection point of the S-shaped function, and the parameter $\lambda \geq 1$ controls its sharpness. In Fig. 2, we illustrate the weighting transform functions corresponding to different R and λ. As can be seen, the weight μ_j is approaching 1 as $A_j \to 0$, and goes to 0 when $A_j \to \pi$. In other words, the weighting transform actually works as a classifier in our WVDF method. According to the aggregated angular distance A_j, the vectors in the filtering window are classified into the most centrally located part and the other part (Fig. 3). The vectors belonging to the most centrally located subset are assigned with large weights and contribute mainly to the filtering result while the other vectors with small weights have little effect on the dip estimation. Herein, the parameter R acts as the threshold and the parameter λ controls the transition between these two parts, where a large λ leads to a sharp transition of the transform function and a small one results in a slow degradation. The two parameters should be chosen in accordance with the data quality. Small R and large λ should be chosen for the data with high signal-to-noise-ratio (SNR) to well discriminate the most centrally located subset while for noisy data a little large R and small λ should be used to include more vector elements to guarantee sufficient smoothing performance.

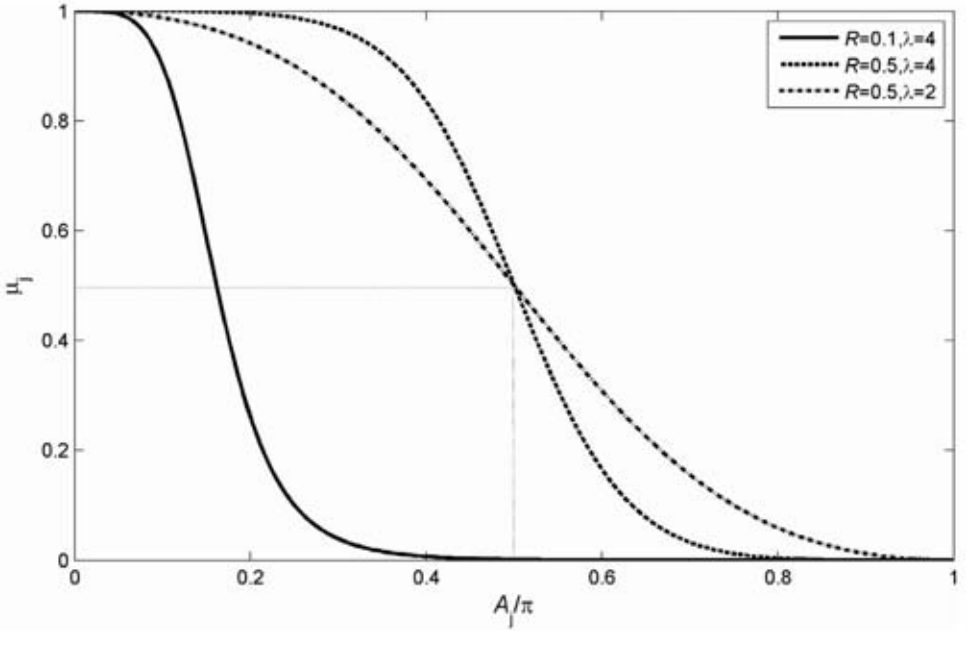

Fig. 2. S-shaped weighting transform functions for the WVDF method.

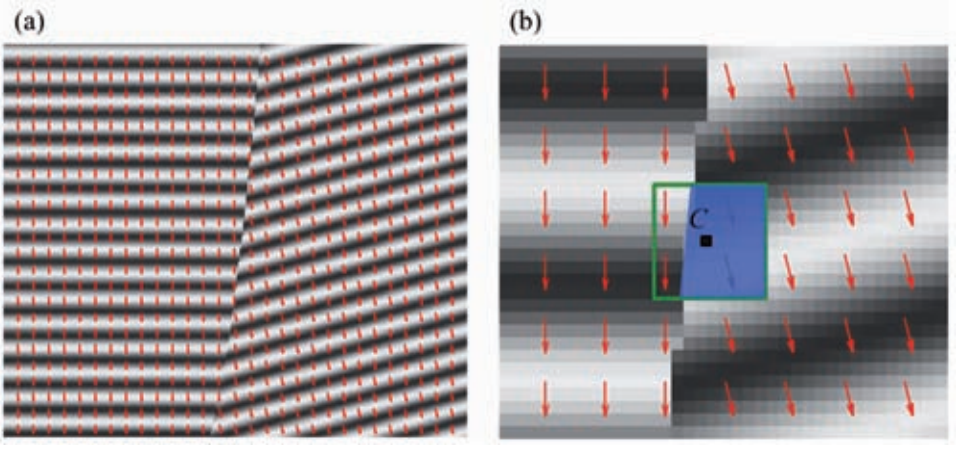

Fig. 3. Schematic showing the filtering performance of the WVDF in the vicinity of a fault. (a) Synthetic model with a fault overlaid red arrows indicating gradients, (b) a zoomed part of (a) in the fault region overlaid a green box indicating an analyzing window centered about the target point C. The blue part denotes large weights and the transparent part denotes very small weights taken by vectors therein.

Comparing with the multiwindow analysis technique used in the dip scan methods (Marfurt, 2006), our WVDF method derives its output from the most centrally located subset chosen adaptively in the analyzing window rather than selects the reflector dip from some predefined subwindow. This is very important for the detection of small discontinuities and subtle features. However, the computational complexity of the WVDF method to process the 3D vector field should be considered. Since the aggregated angular distances have to be computed for all vectors inside the filtering window, the computation burden is mainly dominated by the inner products of vectors. Without loss of generality, let the filtering window be cubic, i.e., $N_x = N_y = N_z = M$. Then, for each filtering window, the total number of vector inner products having to be computed is

$$n_{vip} = M^3(M^3 - 1)/2 \sim O(M^6) \quad . \tag{9}$$

We see that n_{vip} is proportional to M^6 and is a relatively large number. This computation can be reduced because the filtering windows of two adjacent target points have large overlap. $M^2(M - 1)$ inner products are the same and only M^2 are different. So the number of inner products having to be done now becomes

$$n_{vip-r} = M^2(M - 1)M^2 + M^2(M^2 - 1)/2 \sim O(M^5) \quad . \tag{10}$$

Moreover, some simplifications can also be adopted to reduce the computational cost. In this paper, we take the following predigestion: firstly, the vectors in each cuboid filtering window are simply averaged along the z-axis to get a vector field within a square window of size $N_x \times N_y$, and then the WVDF is performed within this 2D window to obtain the final filtering result for the target point. Since seismic data are composed by a stack of layers, the vectors along the z-direction are always oriented closely in the analyzing window. Thus, our predigestion is feasible and acceptable and has little influence on the characterization of lateral discontinuities and subtle features.

SYNTHETIC DATA EXAMPLES

The synthetic data is a 2D section composed by a stack of layers with sinusoidal variation amplitude and broken by a fault [Fig. 4(a)]. The synthetic model is defined by:

$$u(x,z) = \sin[2\pi f(-x\cdot\sin\theta + z\cdot\cos\theta)] \quad , \tag{11}$$

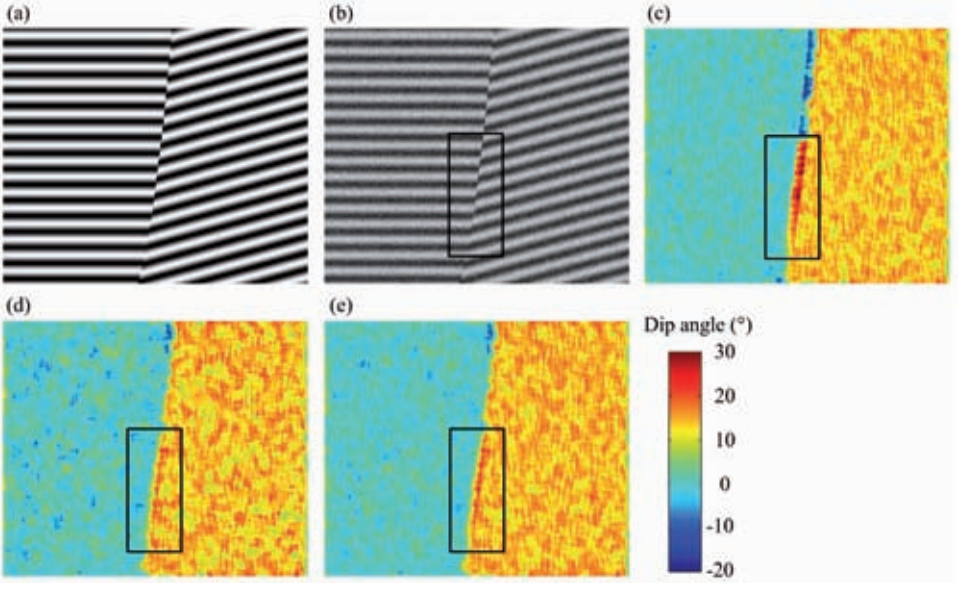

Fig. 4. (a) Original data, (b) noisy data with SNR = 11 dB. Estimated dips by (c) the AMF, (d) the BVDF, and (e) the WVDF methods.

where f is the frequency of the reflection events, and θ corresponds to the dip angle. The left part of our synthesized data is for dip angle $\theta = 0°$ while the right part has $\theta = 15°$. The data are then corrupted with additive Gaussian white noise at different SNR levels of 8dB, 11dB, and 14dB. Fig. 4(b) shows the noisy profile for 11 dB SNR.

We applied the WVDF to smooth the inverted gradient vector field of the noisy synthetic data and assigned parameters $R = 0.1$ and $\lambda = 4$ for the weighting transform function (the solid line in Fig. 2). Besides, the simple AMF and the BVDF methods are presented here for comparison. Every filter is using a square filtering window of size 9×9. The dip estimation results are given both in terms of visual quality and Root-Mean-Square-Error (RMSE), which allows quantifying the similarity between each estimated result and the real dip angle. In order to do detailed comparisons, the original profile is segmented into two regions: faults and non-faults. The segmentation is achieved by simply setting 4 points, which is the distance from the target point to the border in the filtering window, on each side of the discontinuity as fault regions and the other part as non-fault regions. Then, for each estimated result, the RMSE has been computed in these two different zones in order to show the behavior of the methods particularly in the fault regions. The resulting RMSE values are provided in Table 1 and the estimated dips from the noisy profile (SNR = 11dB) are also shown in Figs. 4(c)-(e).

The RMSE results show that both the WVDF and BVDF methods have better performance than the AMF method in fault regions whereas both the WVDF and AMF methods are superior to the BVDF method in non-fault regions. This can also be seen from Figs. 4(c)-(e). The AMF method produces false dip estimates in the fault regions whereas the dip edges located by the

Table 1. RMSE values for different dip estimations of noisy synthetic data in both fault and non-fault regions (50 trials).

Original SNR values (dB)	Methods	RMSE (°)		
		Fault Region	Non-Fault Region	Whole Profile
8.0	AMF	11.90	3.02	3.57
	BVDF	8.36	3.90	4.08
	WVDF	8.11	3.19	3.42
11.0	AMF	13.00	2.02	2.93
	BVDF	7.30	2.72	2.92
	WVDF	7.17	2.06	2.35
14.0	AMF	13.24	1.42	2.60
	BVDF	6.07	1.88	2.11
	WVDF	5.99	1.26	1.59

WVDF and BVDF methods are more accurate (Figs. 5(b)-(d)). On the other hand, both the WVDF and AMF methods produce spatially more consistent dips than the BVDF method in non-fault regions. To the end, considering the smoothing performance and edge preserving ability, our WVDF method takes advantage over both the AMF and BVDF methods.

REAL DATA EXAMPLES

The methodology presented here was applied to a 3D seismic data from the Daqing oil field in China. The data set has a time sampling frequency of 1 kHz, and inline and crossline spacing of 20.0 m. A fault network with several stratigraphic features, such as a major channel and some weak ones, is present in this data. Fig. 6(a) shows the vertical slice along line AA′ through the seismic data. The WVDF and AMF methods with a cubic analyzing window of size $9 \times 9 \times 9$ are used to estimate reflector orientations and the same parameters $R = 0.1$ and $\lambda = 4$ as in the synthetic examples are for the weighting transform function of the WVDF. Besides, the instantaneous dips and the smoothed dips of maximum similarity computed by the commercial software SMT (http://www.seismicmicro.com) are also presented. Figs. 6(b)-(e) depict the estimated dips. The instantaneous phase dips are aliased for steep reflector dips while the smoothed dips of maximum similarity suffer from strip artifacts and are trapped in the vicinities of faults. Both the estimated dips of the AMF

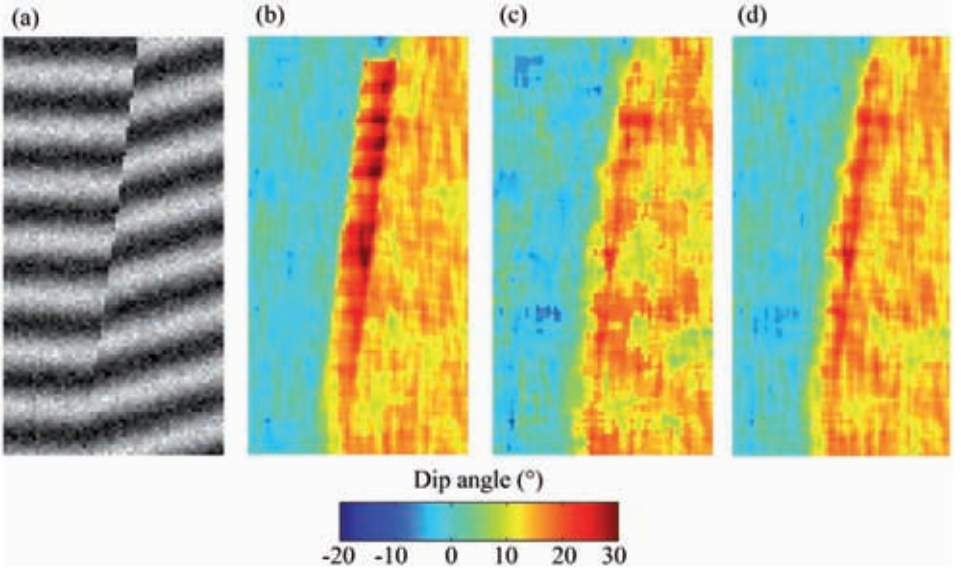

Fig. 5. Zooms of the marked black rectangles in Figs. 4(b)-(e), respectively.

and WVDF methods share a comparatively consistent spatial appearance. However, compared with the AMF method, the proposed WVDF method honors the abrupt changes in dip along the faults. Some typical places are indicated by arrows in Figs. 6(d)-(e). For a further comparison between the WVDF and AMF methods, we calculated the volumetric curvatures directly from the estimated seismic dips and azimuths (al-Dossary and Marfurt, 2006). Figs. 7(d)-(e) show the time slices of the most negative curvature attributes at 0.785s.

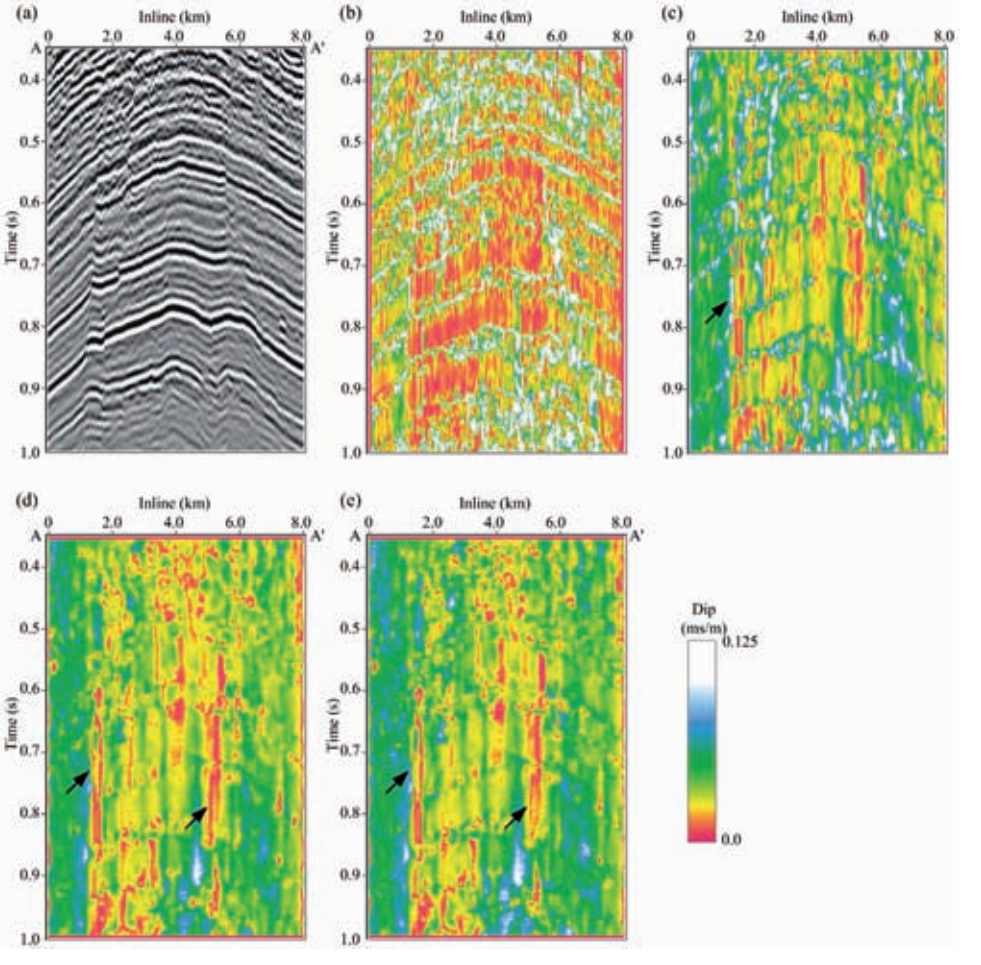

Fig. 6. (a) Vertical slice along line AA' through the seismic data from Daqing oil field. The apparent dips calculated using (b) the instantaneous dip estimation, (c) smoothed dip of maximum similarity over a nine-trace × nine-trace window along local dips, (d) the AMF, and (e) the WVDF methods.

A clearly higher resolution curvature attribute is obtained through the dip and azimuth estimated by our WVDF method and it depicts lateral discontinuities and stratigraphic features more clearly and accurately than the one from the AMF method. Compared with that in Fig. 7(d), the faults in the central left part can be identified more easily from Fig. 7(e) and a fine channel from southeast to northwest in the upper central part also emerges in Fig. 7(e).

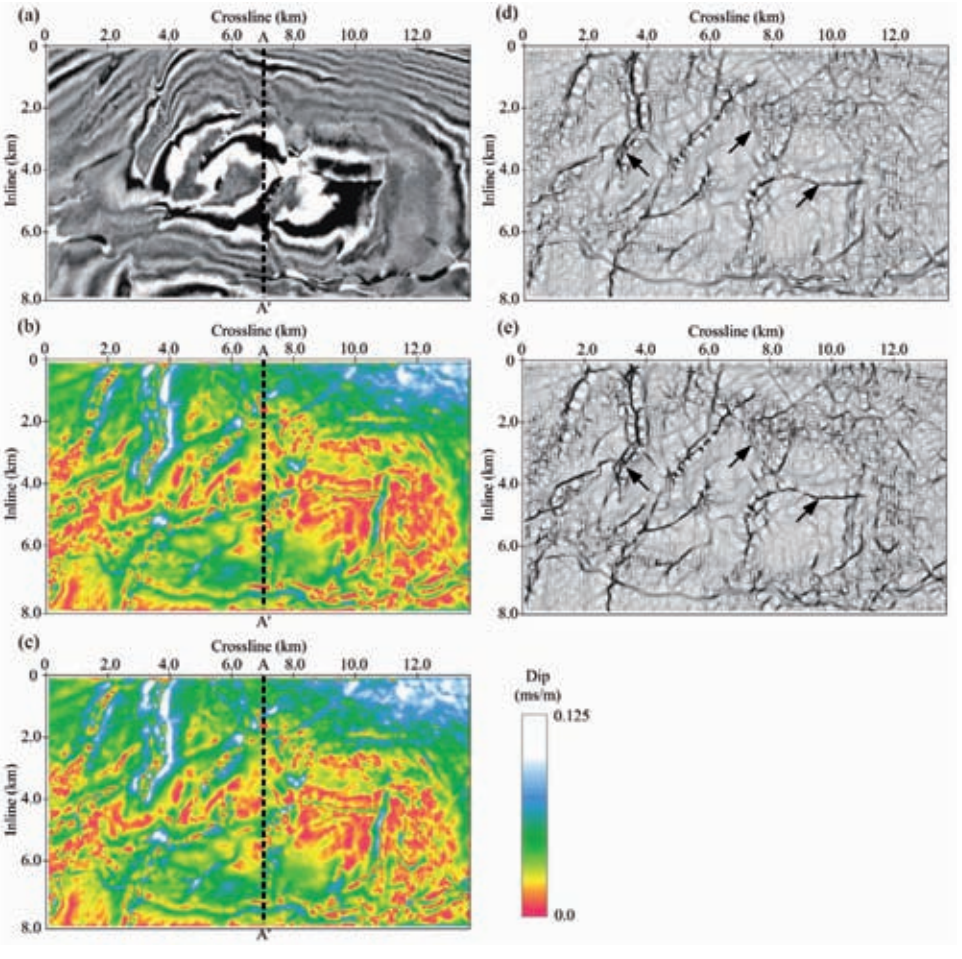

Fig. 7. (a) Time slice at 0.785 s through the original seismic volume. Corresponding slice through apparent dip volumes, calculated using (b) the AMF, and (c) the WVDF methods. Corresponding slice through the most negative curvature attributes volumes with short-wavelength (α = 1.25), calculated from volumetric estimations of dip and azimuth by (d) the AMF, and (e) the WVDF methods.

DISCUSSIONS

The computation of the gradients by low order finite difference such as simple central difference may cause inaccuracy with no consideration about the frequency and orientation contents of structures. Wang et al. (2008b) investigated this problem through their so-called "Enhanced isotropic gradient operators" which is also adopted in this paper. The enhanced gradient operators are derived by first parameterizing corresponding numerical operators, followed by applying them to plane waves to determine the parameters for the operators by matching analytical gradients with numerical gradients. The numerical accuracy against frequency and orientation is minimized by the properly selected parameters. Besides using seismic amplitude data, the raw dips can also be computed from the instantaneous phase. In this case, the gradients should be obtained from analytical traces using a Hilbert transform rather than directly applying the finite-difference method on the instantaneous phase.

The size and aspect ratio of the analyzing window in the WVDF method are depending upon the exploration objectives. Typically, N_x, N_y and N_z range from 3 to 21 can be used to extract meaningful geological features. Generally large analyzing windows lead to spatially more consistent dip and azimuth and are suitable for extracting large-scale features. On the contrary, small analyzing windows are used to obtain high-resolution dip and azimuth for subtle feature detection. If some edge preserving filter is carefully applied to the data previously, small analyzing windows are particularly preferred to integrate information to obtain high-resolution results with less consideration about the noise suppression. In this paper, in order to show the performance of the WVDF method simultaneously for noise suppression and detail feature preservation, we choose a moderate size for the analyzing window, which means 9×9 for the 2D synthetic model and $9 \times 9 \times 9$ for the 3D real data set.

CONCLUSIONS

In this paper, we propose an adaptively weighting vector filter, i.e., the WVDF, for smoothing seismic dip and azimuth calculated by a finite difference method. The WVDF involves both a directional filtering scheme based on aggregated angle distances and the magnitude component of each one of the gradient vectors. Applications on synthetic data show that the WVDF method takes advantage of smoothing performance of the AMF method in non-fault regions and edge-preserving ability of the BVDF method in the vicinities of faults. The real data example demonstrates the excellent behavior of our WVDF method for seismic reflector orientation estimation. With robust estimates of seismic dip and azimuth by our WVDF method, more refined curvature attributes are obtained for seismic interpretation.

ACKNOWLEDGEMENTS

We are grateful to the reviewer Gilles Lambaré for his constructive comments, which allowed us to improve the quality of the manuscript. We would also like to acknowledge the Exploration and Development Research Institute of Daqing Oilfield Company Ltd. for providing 3D seismic data. This research has been partially supported by the National Hi-Tech Research and Development Program of China (under grants 2006AA09A102) and the National Science Fund of China (under grants 40730424 & 40674064).

REFERENCES

AlBinHassan, N.M., Luo, Y. and Al-Faraj, M.N., 2006. 3D edge-preserving smoothing and applications. Geophysics, 71(4): 5-11.

Al-Dossary, S. and Marfurt, K.J., 2006. 3D volumetric multispectral estimates of reflector curvature and rotation. Geophysics, 71(5): 41-51.

Barnes, A.E., 1996. Theory of two-dimensional complex seismic trace analysis. Geophysics, 61: 264-272.

Barnes, A.E., 2000. Weighted average seismic attributes. Geophysics, 65: 275-285.

Dalley, D., 2008. Value of visual attributes: Revisiting dip and azimuth displays for 3D seismic interpretation. First Break, 26: 87-91.

Fehmers, G. and Hocker, C., 2003. Fast structural interpretation with structure-oriented filtering. Geophysics, 68: 1286-1293.

Fomel, S., 2002. Applications of plane-wave destruction filters. Geophysics, 67: 1946-1960.

Gersztenkorn, A. and Marfurt, K.J., 1999. Eigenstructure based coherence computations as an aid to 3D structural and stratigraphic mapping. Geophysics, 64: 1468-1479.

Hoeber, H., Brandwood, S. and Whitcombe, D.N., 2006. Structurally consistent filtering. Extended Abstr., 68th EAGE Conf., Vienna: Z-99.

Lavialle, O., Pop, S., Germain, C., Donias, M., Guillon, S., Keskes, N. and Berthoumieu, Y., 2007. Seismic fault preserving diffusion. J. Appl. Geophys., 61: 132-141.

Lukac, R., Smolka, B., Martin, K., Plataniotis, K.N. and Venetsanopoulos, A.N., 2005. Vector filtering for color imaging. IEEE Signal Proc. Mag., Spec. Issue on Color Image Proc., 22: 74-86.

Luo, Y., Higgs, W.G. and Kowalik, W.S., 1996. Edge detection and stratigraphic analysis using 3D seismic data. Expanded Abstr., 66th Ann. Internat. SEG Mtg., Denver: 324-327.

Luo, Y., Marhoon, M., Al-Dossary, S., and Alfaraj, M., 2002. Edge-preserving smoothing and applications. The Leading Edge, 21: 136-158.

Luo, Y., Wang, Y.E., AlBinHassan, N.M. and Alfaraj, M.N., 2006. Computation of dips and azimuths with weighted structural tensor approach. Geophysics, 71(5): 119-121.

Marfurt, K.J., Kirlin, R.L., Farmer, S.H. and Bahorich, M.S., 1998. 3D seismic attributes using a running window semblance-base algorithm. Geophysics, 63: 1150-1165.

Marfurt, K.J., Sudhaker, V., Gersztenkorn, A., Crawford, K.D. and Nissen, S.E., 1999. Coherence calculations in the presence of structural dip. Geophysics, 64: 104-111.

Marfurt, K.J., 2006. Robust estimates of 3D reflector dip and azimuth. Geophysics, 71(4): 29-40.

Ottolini, R., 1983. Signal/noise separation in dip space. SEP report 37: 143-149.

Randen, T., Monsen, E., Signer, C., Abrahamsen, A., Hansen, J.O., Saeter, T., Schlaf, J. and Sonneland, L., 2000. Three-dimensional texture attributes for seismic data analysis. Expanded Abstr., 70th Ann. Internat. SEG Mtg., Calgary, Alberta: 668-671.

Trahanias, P.E. and Venetsanopoulos, A.N., 1993. Vector directional filters: A new class of multichannel image processing filter. IEEE Trans. Image Proc., 2(4): 528-534.

Wang, Y.E., Luo, Y. and Alfaraj, M., 2008. Inverse-vector approach for smoothing dips and azimuths. Geophysics, 73(6): 9-14.

Wang, Y.E., Luo, Y. and Alfaraj, M., 2008. Enhanced isotropic 2D and 3D gradient method. U.S. Patent 11/787986.